The 13th IEEE International Conference on Control and Automation

Hotel Metropol
Ohrid, Macedonia
3-5 July, 2017

Organised by

IEEE Control Systems Chapter, Singapore

Electronics, Telecommunications, Automatica & Informatics Society, Macedonia

Technically Sponsored by

IEEE Control Systems Society

Technical Committee of Control Theory, Chinese Association of Automation

Stankovski, Mile	SS Cyril and Methodius Univ
Gochev, Ivan	Ss. Cyril and Methodius Univ
Ojleska Latkoska, Vesna	Ss. Cyril and Methodus in Skopje, Faculty of Electrical Engineer

11:30-11:50, Paper MoAT3.4

PDF Collective Adaptation Evolution of Weighted Complex Networks: On Syncronizability Dependence (I)

Jing, Yuanwei	Northeastern Univ
Wang, Dan	Dalian Maritime Univ
Dimirovski, Georgi Marko	Dogus Univ. of Istanbul

11:50-12:10, Paper MoAT3.5

PDF The System Identification in Industrial Control: Case Study on the Differential Wheeled Mobile Robot (I)

Bunjaku, Drilon	Univ. of Mitrovica "Isa Boletini"
Stankovski, Mile	SS Cyril and Methodius Univ

12:10-12:30, Paper MoAT3.6

PDF Online Learning and Inference Based Flight Envelope Estimation for Aircraft Loss-Of-Control Prevention (I)

Zhou, Hang	Beihang Univ
Yang, Lingyu	Beihang Unviersity
Zhang, Jing	Beihang Univ
Yang, Xiaoke	Beihang Univ

MoAT4	Ohrid hall
Signal Processing & Sensor/Data Fusion	Regular Session
Chair: Balchanos, Michael	Georgia Inst. of Tech
Co-Chair: Amosov, Oleg S.	Komsomolsk-On-Amur State Tech. Univ

10:30-10:50, Paper MoAT4.1

PDF Hybrid Orientation Filter Aided Indoor Tracking for Pedestrians Using a Smartphone

Yang, Zhe	Zhejiang Univ
Pan, Yun	Zhejiang Univ
Zhang, Ling	Zhejiang Univ

10:50-11:10, Paper MoAT4.2

PDF Single-Channel Speech Separation Based on Robust Sparse Bayesian Learning

Wang, Zhe	NanyangTechnologicalUniversity
Bi, Guoan	Nanyang Tech. Univ
Li, Xiumei	School of Information, Science and Engineering, HangZhouNormal U

11:10-11:30, Paper MoAT4.3

PDF Wavelet Based Filtering of Mobile Object Fractional Trajectory Parameters

Amosov, Oleg S.	Komsomolsk-On-Amur State Tech. Univ
Baena, Svetlana G.	Komsomolsk-On-Amur State Tech. Univ

11:30-11:50, Paper MoAT4.4

2017 13th IEEE International Conference on Control & Automation (ICCA)
July 3-6, 2017. Ohrid, Macedonia

Online Learning and Inference Based Flight Envelope Estimation for Aircraft Loss-of-Control Prevention

Hang Zhou, Lingyu Yang, Jing Zhang, and Xiaoke Yang

Abstract— **Aircraft loss-of-control (LOC) is the major contributing factor to fatal accidents and is characterised by the manoeuvring of aircraft beyond the allowable flight envelopes. This paper proposes an online learning and inference based method for aircraft flight envelope estimation in order to prevent aircraft LOC. The lift and drag coefficients of the aircraft are identified online using an extended Kalman filter and the aircraft flight dynamics. A Gaussian process regression model then learns and infers the up-to-date form of the lift curve from both prior knowledge and the identification data. The extremum of the inferred lift curve, including the maximum lift coefficient and the critical angle of attack are used to compute the flight envelope estimate of the aircraft. Numerical simulation on the NASA generic transportation model (GTM) shows that the proposed method can effectively estimate the aircraft lift and drag coefficients, and by using the extremum on the up-to-date lift curve inferred, return the flight envelope under a wingtip impairment condition.**

Index Terms— **loss of control, flight envelope estimation, Gaussian process regression, extended Kalman filter, Generic Transportation Model**

I. Introduction

With advanced instrumentation, the fly-by-wire (FBW) control system, and various fault-tolerant design, the probability of flight accidents on modern aircraft has been significantly reduced. Yet modern aircraft are still not immune to accidents or incidents, as summarised by the Boeing company in the survey of commercial jet airplane accidents these years[1]. Despite various causes, such as mechanical failure, "spatial disorientation", "undetected loss of airspeed"[2], etc., flight accident, especially fatal ones, are mostly a direct consequence of loss-of-control (LOC). LOC has been the major contributing factor to fatal accidents, among others like controlled flight into terrain and runway excursion, etc.[3].

LOC refers to the manoeuvring of the aircraft beyond its allowable normal flight envelopes, including the angle of attack and the sideslip angle, the attitude, and the airspeed, etc., which may lead to nonlinearity in the aerodynamics and flight dynamics, or cause problems to the aircraft structural integrity[4]. Untended development of LOC will further cause the aircraft to rapidly enter into stall or spin. Due to the critical position of the flight envelope to LOC, the FBW system on modern aircraft has been designed with various protection functionalities, such as the angle of attack and bank angle protections on Airbus aircraft[5], to suppress the control inputs which may push the aircraft out of the normal operating envelope. In spite of the success of these efforts, aircraft are still susceptible to various unusual situations, such as the failure of control surfaces, damage to the aircraft structure, adverse weather conditions, etc., in which either the force and torque generating capability of the control surfaces decreases, or the aerodynamics and flight dynamics the whole aircraft changes. The normal safe flight envelope in these situations may be compromised, with unachievable and possibly LOC-inducing regions.

As the flight envelope protection functionality restrains the control inputs, a supervision procedure is desirable for the envelope itself. This procedure monitors abnormal situations or unusual changes in aircraft characteristics, and adaptively updates the envelope protection boundary. The core to such a procedure is the estimation of the envelop, and research effort on this topic is summarised briefly as follows.

Reference [6] presents an extensive coverage of an adaptive flight envelope estimation and protection method for aircraft with both actuator faults and structural damages. The actuator faults are identified by a bank of nonlinear fault detection and isolation filters, while changes in aircraft aerodynamic coefficients due to damage conditions are modelled by unknown additive terms and identified with a linear regression method. The envelope protection is achieved through the inverse of an artificial neural networks model of the aircraft dynamics for command margins against the limits.

Reference [7] proposes an upset detection and physical modelling based flight envelope estimation method as an outer "supervisory" loop for the existing envelope limiting control systems. The impact of degradation, including stall characteristics and lifting surface damage effects, on the overall aircraft performance and operational limits is determined offline using an analytical approach incorporating aircraft geometric parameters and sectional aerodynamic data. The integration of these two blocks leads to the final onboard envelope determination function.

Reference [8] covers an in-depth investigation of the envelope estimation problem for impaired aircraft. Detailed *a priori* modelling and analysis of the inertial, structural, and aerodynamics characteristics of the impaired aircraft is discussed, leading to a parameterised representation of the damages. An extended Kalman filter combined with a differential vortex lattice method is then proposed for the estimation of the impairment parameters. The estimated parameters are used to infer the damage conditions, upon

This work was supported by the National Natural Science Foundation of China (Grant No. 61304030 and 61273099).

Hang Zhou, Lingyu Yang, Jing Zhang, and Xiaoke Yang are with the School of Automation Science and Electrical Engineering, Beihang University, Beijing, 100191, China. email: hangzhou@buaa.edu.cn, yanglingyu@buaa.edu.cn, zhangjing2013@buaa.edu.cn, dr.x.yang@ieee.org.

which the stall angle of attack is obtained via local strip lift coefficient analysis. The aircraft performance envelope is then computed as functions of the maximum angle of attack.

References [9], [10], and [11] propose a reachability-analysis-based method for aircraft manoeuvring envelope estimation. Dynamics of the unknown aerodynamic parameters (random walk) is augmented into the aircraft longitudinal manoeuvring model. A maximum a posteriori estimator is used to estimate the parameters, upon which the aircraft trim envelope is obtained on a grid of state values. The aircraft manoeuvring envelope is then computed via a bi-directional reachability analysis from the trim envelope using an optimal control formulation.

In this paper, a novel online learning-based flight envelope estimation approach is proposed. The overall structure of the proposed approach is similar to most references, containing a parameter identification procedure combined with an envelope determination one. Unlike [7] and [8], in which parameterised faults or performance degradation parameters are identified, our proposed method identifies the aerodynamic coefficients directly, which is similar to reference [11]. The method of estimating the flight envelope in this paper is novel and distinct from existing literature, in that a Gaussian process (GP) regression model is utilised to represent the lift coefficient curve. The GP model is a probabilistic function approximator, which effectively fuses prior knowledge and the identified parameters data in a Bayesian way, giving an estimate of the whole lift curve. The flight envelope is then computed from the extremum of the estimated lift curve. This procedure draws inspiration from [6], [7], and [8], in which other ways of integrating prior knowledge, or offline analysis with online identification are discussed. The merit of the GP regression model lies in its flexibility and learning capability. The flexibility allows it to accept various types of prior knowledge, and the learning capability to learn from online identified data.

The rest of this paper is organised as follows. Section II reviews some of the preliminary background knowledge. Section III covers the main method, including the parameter identification and the GP regression model-based envelope estimation methods. A case study on the NASA generic transportation model (GTM) is analysed in section IV, followed by conclusions and further work in section V.

II. Background Knowledge

A. Aircraft Aerodynamics and Flight Dynamics

Flight dynamics of a fixed-wing aircraft is usually described by a 6 degree-of-freedom rigid body equations of motion. Due to the symmetry of the aircraft geometry, under level and zero sideslip flight condition, the longitudinal and lateral motions can be decoupled. Dynamics of two selected longitudinal variables, the true airspeed V and the angle of attack (AoA) α, is

$$\dot{V} = \frac{T}{m}\cos\alpha - \frac{D}{m} - g\sin(\theta-\alpha), \tag{1a}$$

$$\dot{\alpha} = -\frac{T}{mV}\sin\alpha - \frac{L}{mV} + q + \frac{g}{V}\cos(\theta-\alpha), \tag{1b}$$

where m is the mass of the aircraft, g is the gravitational acceleration, θ is the pitch angle, q is the pitch rate, and T is the engine thrust. The two aerodynamic forces, lift L and drag D can be further written as

$$L = \frac{1}{2}\rho V^2 S C_L, \tag{2a}$$

$$D = \frac{1}{2}\rho V^2 S C_D, \tag{2b}$$

where C_L and C_D are the lift coefficient and drag coefficient, respectively, and S is the reference area.

B. Gaussian Process Regression Model

A Gaussian process (GP) defines a distribution over functions[13]. By providing a probabilistic description of a function $y = f(\mathbf{x}) : \mathbb{R}^n \mapsto \mathbb{R}$, a GP can inherently perform nonlinear regression through Bayes rule and input-output data. A Gaussian process regression model for function $f(\mathbf{x})$ is usually denoted as

$$f(\mathbf{x}) \sim \mathcal{GP}(m(\mathbf{x}), k(\mathbf{x},\mathbf{x}')), \tag{3}$$

where $m(\mathbf{x})$ is the mean function, and $k(\mathbf{x},\mathbf{x}')$ is the covariance function with $\mathbf{x}$, $\mathbf{x}' \in \mathbb{R}^n$ being two input points. The mean function depicts the 'average shape' of the function, while the covariance function reflects the 'variance' by specifying the covariance between two points on the function computed from the inputs.

Given an input-output data set $\mathcal{D} = \{\mathbf{X},\mathbf{y}\}$, the regression result, or the posterior GP, is

$$f(\mathbf{x}) \sim \mathcal{GP}(m_+(\mathbf{x}), k_+(\mathbf{x},\mathbf{x}')), \tag{4}$$

where

$$m_+(\mathbf{x}) = m(\mathbf{x}) + k(\mathbf{x},\mathbf{X})k(\mathbf{X},\mathbf{X})^{-1}\left(\mathbf{y} - m(\mathbf{X})\right), \tag{5a}$$

$$k_+(\mathbf{x},\mathbf{x}') = k(\mathbf{x},\mathbf{x}') - k(\mathbf{x},\mathbf{X})k(\mathbf{X},\mathbf{X})^{-1}k(\mathbf{X},\mathbf{x}'). \tag{5b}$$

Parameters $\boldsymbol{\theta}$ in the mean and the covariance functions are called the hyper-parameters of the GP, and is usually trained by minimising the negative logarithm marginal likelihood $-\log p(\mathbf{y}|\mathbf{X})$, i.e.

$$\begin{aligned}\hat{\boldsymbol{\theta}} \in \arg\min_{\boldsymbol{\theta}} \frac{1}{2}(\mathbf{y}-\mathbf{m}_{\boldsymbol{\theta}})^\top \mathbf{K}_{\boldsymbol{\theta}}^{-1}(\mathbf{y}-\mathbf{m}_{\boldsymbol{\theta}}) \\ + \frac{1}{2}\log|\mathbf{K}_{\boldsymbol{\theta}}| + \frac{1}{2}n\log(2\pi),\end{aligned} \tag{6}$$

where $\mathbf{K}_{\boldsymbol{\theta}} = k(\mathbf{X},\mathbf{X})$, $\mathbf{m}_{\boldsymbol{\theta}} = m(\mathbf{X})$.

III. Learning and Inference Based Flight Envelope Estimation

As stated in the introduction, the main prologue to aircraft LOC is the deviation of its states beyond the safe flight envelope. Existing envelope protections in the FBW control system is based on the normal aircraft characteristics, which may well have been changed in LOC-prone adverse conditions, such as icing and structural damages. An adaptive online envelope estimation procedure is thus desirable, in order to provide an up-to-date estimate of the envelope boundaries.

In this section, the proposed learning-based flight envelope estimation scheme is discussed in detail. As shown in the block diagram in Fig. 1, the proposed scheme consists of an extended Kalman filter (EKF), an online learning and inference block with a Gaussian process regression (GPR) model, and a flight envelope computation block. The EKF takes flight parameters from the aircraft and produces an estimate of the current lift coefficient. The online learning and inference block collects the lift coefficient estimate and fuses the data with prior knowledge through a GPR model, generating an approximation of the lift curve. The maximum lift coefficient on the curve is then used for the flight envelope computation, results of which can be shown in the primary flight display as an assistance to the pilot.

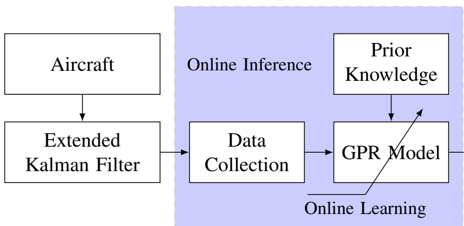

Fig. 1: Block diagram of the proposed online learning and inference based flight envelope estimation method.

A. Aircraft Aerodynamic Coefficients Estimation

In Section II-A, dynamics of the aircraft true airspeed V and the angle of attack α are listed in (1a) and (1b), coupled with the lift coefficient C_L and the drag coefficient C_D. In order to estimate these coefficients, a random walk assumption is put over their dynamics, i.e.

$$\dot{C}_D = w_{C_D}, \tag{7a}$$
$$\dot{C}_L = w_{C_L}, \tag{7b}$$

where w_{C_L} and w_{C_D} are two zero-mean Gaussian random variables. (7a) and (7b) are then appended to the longitudinal dynamics (1a) and (1b), forming an augmented system in a compact form as

$$\dot{\mathbf{x}} = \mathbf{f}(\mathbf{x}, \mathbf{u}) + \mathbf{w}, \tag{8a}$$
$$\mathbf{z} = \mathbf{h}(\mathbf{x}) + \mathbf{v} = \mathbf{H}\mathbf{x} + \mathbf{v}, \tag{8b}$$

where the state $\mathbf{x} = \begin{bmatrix} V & \alpha & C_D & C_L \end{bmatrix}^\top$, the output $\mathbf{z} = \begin{bmatrix} V & \alpha \end{bmatrix}^\top$. A virtual or exogenous input is defined as $\mathbf{u} = \begin{bmatrix} T & \theta & q \end{bmatrix}^\top$. $\mathbf{w} \sim \mathcal{N}(\mathbf{0}, \mathbf{Q})$ is the process noise, $\mathbf{v} \sim \mathcal{N}(\mathbf{0}, \mathbf{R})$ is the measurement noise. The output function $\mathbf{h}(\mathbf{x})$ is linear with an output matrix of

$$\mathbf{H} = \begin{bmatrix} 1 & 0 & 0 & 0 \\ 0 & 1 & 0 & 0 \end{bmatrix}. \tag{9}$$

Due to the nonlinearity of function $\mathbf{f}$ in $\mathbf{x}$, an extended Kalman filter is needed for the estimation of the augmented state. Linearisation of $\mathbf{f}$ with respect to $\mathbf{x}$ gives

$$\frac{\partial \mathbf{f}(\mathbf{x}, \mathbf{u})}{\partial \mathbf{x}} = \mathbf{F}(\mathbf{x}, \mathbf{u}). \tag{10}$$

Furthermore, the continuous-time dynamics of the augmented system is discretised, and a first-order approximation of the zero-order hold (ZOH) method gives

$$\mathbf{f}_d(\mathbf{x}_k, \mathbf{u}_k) = \mathbf{x}_k + \mathbf{f}(\mathbf{x}_k, \mathbf{u}_k) T_s, \tag{11a}$$
$$\mathbf{F}_d(\mathbf{x}_k, \mathbf{u}_k) = \mathbf{I} + \mathbf{F}(\mathbf{x}_k, \mathbf{u}_k) T_s, \tag{11b}$$
$$\mathbf{Q}_d = \mathbf{Q} T_s, \tag{11c}$$

where k is the time step, and T_s is the sampling period.

The EKF then follows the classic prediction-update mechanism, with prediction equations as

$$\hat{\mathbf{x}}_k^- = \mathbf{f}_d(\hat{\mathbf{x}}_{k-1}, \mathbf{u}_{k-1}), \tag{12a}$$
$$\hat{\mathbf{P}}_k^- = \mathbf{F}_d(\hat{\mathbf{x}}_{k-1}, \mathbf{u}_{k-1}) \hat{\mathbf{P}}_{k-1} \mathbf{F}_d(\hat{\mathbf{x}}_{k-1}, \mathbf{u}_{k-1})^\top + \mathbf{Q}_d, \tag{12b}$$

and update equations as

$$\mathbf{K}_k = \hat{\mathbf{P}}_k^- \mathbf{H}^\top (\mathbf{H} \hat{\mathbf{P}}_k^- \mathbf{H}^\top + \mathbf{R})^{-1}, \tag{13a}$$
$$\hat{\mathbf{x}}_k = \hat{\mathbf{x}}_k^- + \mathbf{K}_k (\mathbf{z}_k - \mathbf{H} \hat{\mathbf{x}}_k^-), \tag{13b}$$
$$\hat{\mathbf{P}}_k = (\mathbf{I} - \mathbf{K}_k \mathbf{H}) \hat{\mathbf{P}}_k^-. \tag{13c}$$

The estimated lift and drag coefficients are embedded in $\hat{\mathbf{x}}_k$.

B. Aircraft Lift Curve Estimation

Since the flight envelope parameters discussed later only depends on the aircraft lift characteristics, the estimated drag coefficient is not used and only the lift curve estimation is discussed in this part.

1) GPR Model of the Lift Curve: Aircraft lift curve (as shown in Fig. 2) is a plot of the lift coefficient C_L against the angle of attack α. Describing a nonlinear mapping from α to C_L, the lift curve can be readily modelled by a Gaussian process as $C_L(\alpha) \sim \mathcal{GP}(m(\alpha), k(\alpha, \alpha'))$.

A variety of mean functions can be used in a GP, such as the zero or the linear mean functions, depending on the prior information to be incorporated. For $C_L(\alpha)$, the mean function is chosen to be

$$m(\alpha) = c_h C_{Lm}(\alpha + a_h) + b_h, \tag{14}$$

where a_h, b_h, and c_h are the hyper-parameters, $C_{Lm}(\alpha)$ is a function describing the *a priori* shape of the lift curve. Fig. 2 depicts the physical meanings of these variables.

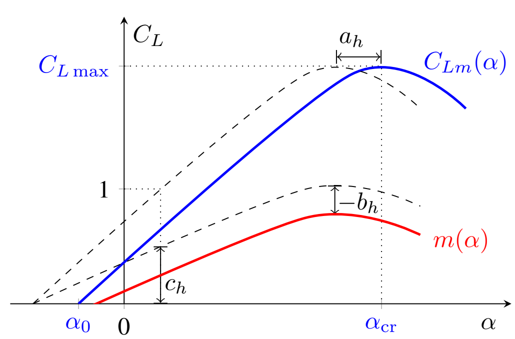

Fig. 2: The mean function of the GPR model $C_L(\alpha)$ and the meaning of its hyper-parameters.

In Fig. 2, $C_{Lm}(\alpha)$ has the shape of a typical lift curve, with a linear section at small angles of attack, and an extremum corresponding to the maximum lift coefficient $C_{L\max}$ and the critical or stall angle of attack α_{cr}. In practice, $C_{Lm}(\alpha)$ can be chosen as the lift curve of the nominal aircraft obtained from wind tunnel experiments. a_h is a horizontal shift parameter, accounting for changes in the critical angle of attack. c_h is a scaling factor adjusting the whole lift curve proportionally, while leaving the zero lift angle of attack α_0 unaffected. b_h is a vertical shift parameter describing additive changes in the lift coefficient. The combination effects of the hyper-parameters a_h, b_h, and c_h are depicted in Fig. 2, which shows both decreased lift coefficients and a reduced stall angle of attack in $m(\alpha)$ as compared with the nominal curve $C_{Lm}(\alpha)$.

Difference between the actual lift curve and the mean function is accounted for by the covariance function of the GPR model. The following sum of a exponentiated quadratic function and an additive noise term is chosen as the covariance function for $C_L(\alpha)$, i.e.

$$k(\alpha, \alpha') = \sigma_f \exp\left[-\frac{(\alpha - \alpha')^2}{2\lambda^2}\right] + \sigma_n^2, \tag{15}$$

where λ, σ_f, and σ_n are the hyper-parameters, representing the input length scale, the 'size' of the difference, and the 'size' of the noise, respectively. This covariance function is capable of describing any smooth function with additive Gaussian noises.

2) Online Learning: By fixing the mean and the covariance functions, prior knowledge has been incorporated into the GPR model. But the hyper-parameters in those functions still need to be determined, in order to effectively fit the model to the data obtained. For the GPR model of $C_L(\alpha)$, the data comes from the estimated lift coefficient by the EKF. The learning of the hyper-parameters are preformed by eq. (6) through a nonlinear optimisation procedure, and is carried out online when there is new data available.

3) Online Inference: After the data are stored and the hyper-parameters learned, the GPR model provides an optimal fusion of the prior knowledge and the current data available. A probabilistic approximation of the current lift curve containing both the mean and the variance can then be inferred from the model by eq. (5a) and (5b). The extremum of the curve can thus be determined, including the critical angle of attack α_{cr} and the maximum lift coefficient $C_{L\max}$.

4) Example: Aircraft Icing: In this part, the GPR model-based lift curve estimation method is tested specifically on an aircraft icing condition. Icing refers to the formation of various types of ice on aircraft's surfaces, e.g. the wing and the control effectors. Icing distorts the airflow over the surfaces, decreasing the aircraft's lift and reducing its stall angle of attack. This example uses the icing data from reference [14]. The lift curves of the nominal clean aircraft together with that of an icing condition are reproduced in Fig. 3.

A GPR model for the lift curve as described above is constructed. The lift curve in clean condition serves as the

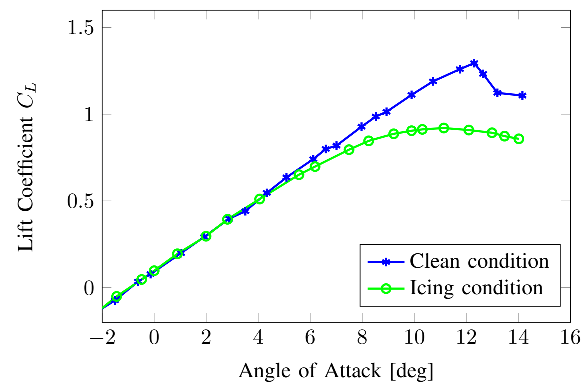

Fig. 3: Lift curves in clean and icing conditions reproduced from reference [14].

$C_{Lm}(\alpha)$ term in the mean function of the GP, with the data point at 14 degrees of AoA removed for the convenience of computing the extremum, as shown in Fig. 4. For the online learning of the hyper-parameters, the upper and lower bounds as listed in Table I are applied. Note that $b_h = 0$ is used in the table since we found that by setting it to be 0, various local optima were avoided and the optimisation performance was improved. Synthetic data are generated by resampling of the spline-interpolated lift curve in icing condition with additive zero-mean Gaussian noises. The variance of the noise is 0.015. Four data sets are tested, with the range of AoA as $[0, 3]$, $[0, 6]$, $[0, 9]$, $[0, 11]$ degrees, respectively.

The mean of the lift curve inferred by the GPR model on these four data sets are shown in Fig. 4, and the corresponding learned hyper-parameters are listed in Table I.

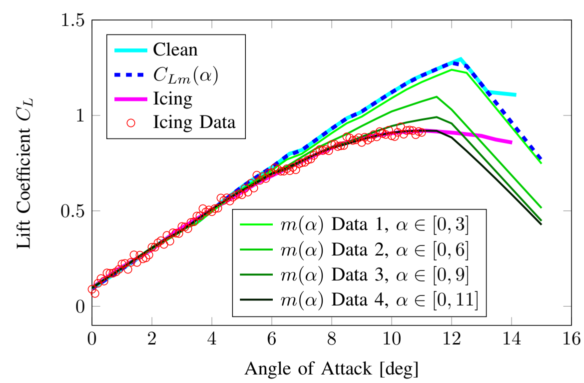

Fig. 4: Lift curves in icing condition as inferred by the GPR model from four sets of icing data. The curves are represented by thin green lines, with deeper colour indicating more data points used.

In Fig. 4, it can be seen that on data set 1, not much difference could be told between the lift curves of clean and icing conditions when the AoA is in between 0 and 3 degrees. The inference of the GPR model lies in line with the clean condition, having slight differences. On data set 2, when the data covers up to 6 degrees of AoA, difference between the lift curves of the two conditions can already be observed. The inferred curve deviates from the prior and approaches

TABLE I: Bounds on the hyper-parameters and the learned values from the four data sets.

Item	a_h	b_h	c_h	λ	σ_f	σ_n
L. Bound	0	0	0.1	10	0.1	1e-4
U. Bound	10	0	1	100	1	0.1
Data 1	0	0	1	100	0.1	0.018
Data 2	0.7	0	0.8	10	0.1	0.018
Data 3	0.6	0	0.7	10	0.2	0.016
Data 4	0.6	0	0.5	10	0.4	0.016

to the one in icing condition. On data sets 3 and 4, as the data reach larger ranges of AoA, the inferred lift curves get closer to the true one in icing condition.

From Table I, firstly it can be seen from the last column that noise in the data is effectively captured by the hyper-parameter σ_n with a value close to 0.015. The values of the hyper-parameters of the mean function indicate that the curve in icing condition is a combination of horizontal shift and proportionally scaling of the clean lift curve.

Fig. 5 and 6 show the estimate of the maximum lift coefficient and the critical AoA from the inferred lift curves on the four data sets. It can also be seen that as more data are obtained, the estimate get closer to the actual extremum. The critical AoA is also estimated before the aircraft stalls.

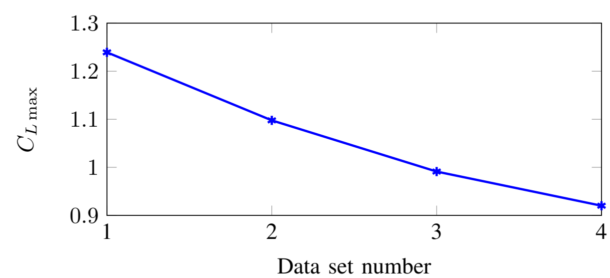

Fig. 5: Estimate of the maximum lift coefficient in icing condition by the GPR model on the four data sets. The true value is around 0.9.

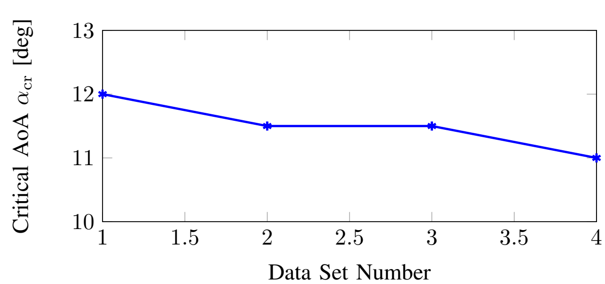

Fig. 6: Estimate of the critical AoA in icing condition by the GPR model on the four data sets. The true value is around 11 degrees.

5) Discussion on the Flexibility of the GPR Model: Since the learning and inference capability of the GPR model derives from Bayes law, it naturally incorporates prior information and data. The flexibility of such a lift curve estimate method lies in both the form of the prior and the data. For instance, the nominal lift curve can be chosen as the prior as in the example above. But if there are other offline analysis or experiment results on the lift curves of various situations, the prior of the GP could be readily changed to any of them, and the switching of the prior can be triggered by a signal from an online fault diagnosis procedure or from sensor measurements. The prior gives the GPR model a starting point and a suitable one could save data acquisition and learning time. Further flexibility comes from the data. By leaving open the source of the data, the GPR model also accepts data of direct measurement or other estimators, not necessarily estimate from an EKF as in the proposed scheme.

C. Aircraft Flight Envelope Computation

Based on the maximum lift coefficient $C_{L\max}$ and the critical angle of attack α_{cr} estimate returned by the GPR model, onboard computation of the flight envelope can be conducted, including bounds for the minimum calibrated airspeed $V_{\mathrm{CAS_{min}}}$, the maximum load factor $n_{z_{\max}}$, and the maximum bank angle $\phi_{\max}$, as suggested by reference [15].

The minimum calibrated airspeed $V_{\mathrm{CAS_{min}}}$ is given by

$$V_{\mathrm{CAS_{min}}} = \sqrt{\frac{2n_z W}{C_{L_{\max}}\rho_0 S}}, \tag{16}$$

where ρ_0 is the air density at sea level, W is the weight of the aircraft, n_z is the load factor.

The maximum load factor $n_{z_{\max}}$ is calculated by

$$\begin{aligned}\Delta n_{z_{\max}} = & \frac{\rho V^2 S C_{L_{\max}}}{2W}\cos\phi - n_Y \sin\phi \\ & -\cos\gamma + \frac{T}{W}\sin\alpha\cos\phi,\end{aligned} \tag{17}$$

where ϕ is the bank angle, n_Y is the lateral load factor, and γ is flight path angle.

The maximum bank or roll angle is

$$\phi_{\max} = \pm\arccos\left(\frac{m(g\cos\gamma + V\dot{\gamma})}{T\sin\alpha + \frac{1}{2}\rho V^2 S C_{L_{\max}}}\right) \tag{18}$$

where m is the aircraft mass, and $\dot{\gamma}$ is the time derivative of the flight path angle.

IV. Case Study: the Impaired Aircraft

A. Impaired Aircraft and Lift Coefficient Analysis

In this section, the proposed flight envelope estimation method is investigated with a case study on a nonlinear simulation model of an impaired aircraft, the generic transportation model (GTM) from NASA[16].

The GTM includes 6 damage conditions, among which two involve noticeable changes in the lift characteristics, namely the left wingtip off and the left stabiliser off conditions. The left wingtip off damage is selected for this case study due to the intactness the pitch control surfaces. The lift curves of the nominal and the damaged aircraft in this condition are plotted in Fig. 7.

It can be seen that both lift curves are linear at small AoA, and nonlinearity starts to appear when the AoA goes beyond 10 degrees. The GTM itself is capable of simulating

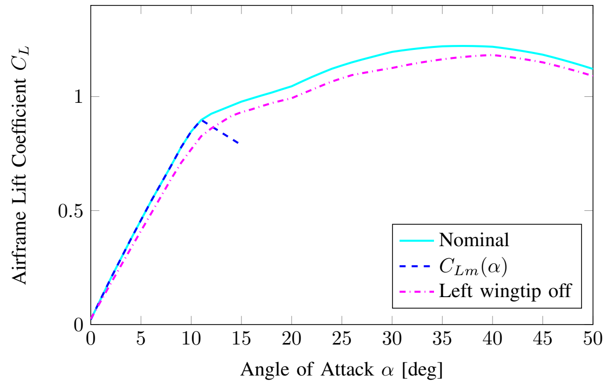

Fig. 7: Aircraft lift curves in nominal and left wingtip off damage conditions.

aircraft stall and post-stall characteristics, while for envelope estimation and protection, our aim is to prevent the aircraft from entering the nonlinear region for increased difficulties in control. Thus, the lift coefficient at 11 degrees of AoA is considered the 'maximum' lift coefficient, rather than the one at around 35 degrees. A GPR model is constructed for the lift curve. The $C_{Lm}(\alpha)$ function as shown in Fig. 7 is used in the mean function to serve as the prior information. For the convenience of computing the extremum, the $C_{Lm}(\alpha)$ function follows the nominal lift curve in the linear section and goes down right after the critical angle of attack.

B. Simulation Scenario

In the case study, a 20-second simulation is carried out. The aircraft starts from a trimmed straight and level flight at 800 feet of altitude and 95 knots of equivalent airspeed. In order to obtain data for a range of AoA, a sinusoidal command is issued to the elevator. A preliminary roll controller was adopted to keep the aircraft at roughly level flight. The aircraft is in nominal condition for the first 10 seconds of the simulation, and suffers from left wingtip off damage for the next 10 seconds.

The time history of the elevator deflections and the AoA is shown in Fig. 8. Changes can be clearly seen at 10 seconds in Fig. 8b, reflecting the damage effects.

C. Simulation Result

The estimation of the lift and drag coefficients from the EKF, together with the true values, are shown in Fig. 9. It can be seen that the EKF accurately estimates both derivatives.

The critical angle of attack α_{cr} and the maximum lift coefficient $C_{L\,\max}$ computed from the GPR model of the lift curve are shown in Fig. 10. The learning and inference of the model take place every one second. It can be seen from Fig.10a that the estimate of the critical AoA wiggles around 10 degrees, which is 1 degree less than than the true value. The estimated maximum lift coefficients as shown in Fig. 10b are also close to the true values, with an apparent decrease after the wingtip damage at 10 seconds. The estimate gets closer to the true values as more data are obtained.

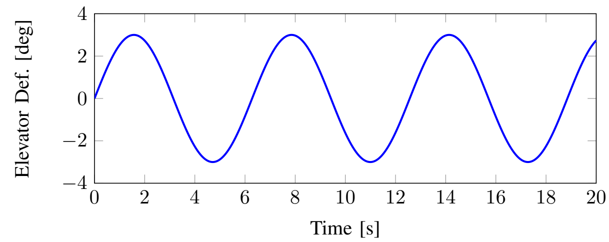

(a) Elevator deflections.

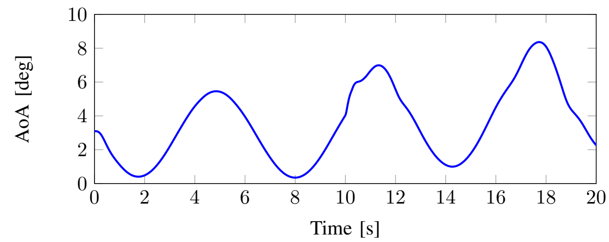

(b) Angle of attack

Fig. 8: Aircraft elevator deflections and angle of attack in the simulation.

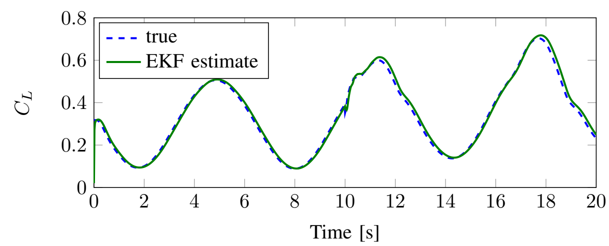

(a) Lift coefficient estimate

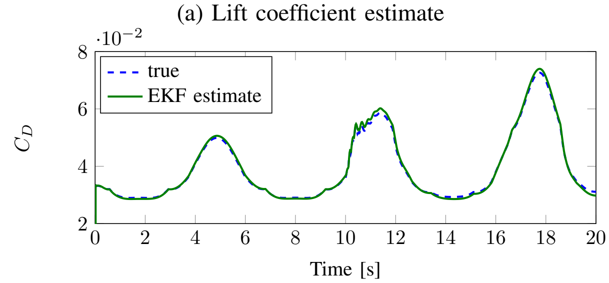

(b) Drag coefficient estimate

Fig. 9: Lift and drag coefficients estimate from the EKF, along with the true values.

The flight envelope estimation by the proposed method is shown in Fig. 11, along with the true values computed from the actual maximum lift coefficients. Despite some errors, it can also be seen that estimated envelopes are close to the true ones, indicating the effectiveness of the proposed method.

V. Conclusions

This paper investigates an online learning and inference based flight envelope estimation method. A Gaussian process regression model learns the up-to-date shape of the lift curve from both prior information and the lift coefficient data identified by an extended Kalman filter. The extremum of the learned lift curve is used to compute the flight envelope.

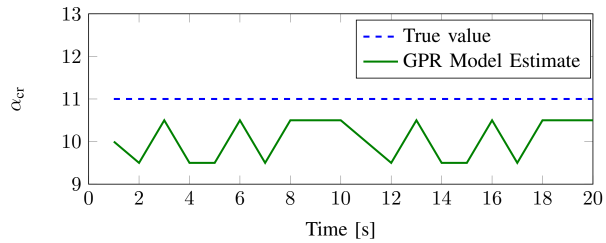

(a) Critical AoA estimate

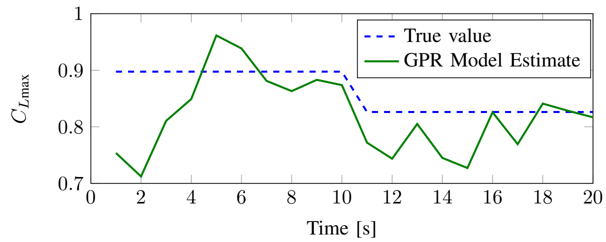

(b) Maximum lift coefficient estimate

Fig. 10: Critical AoA and maximum lift coefficient estimate from the GPR model of the lift curve, with a 1-second update interval.

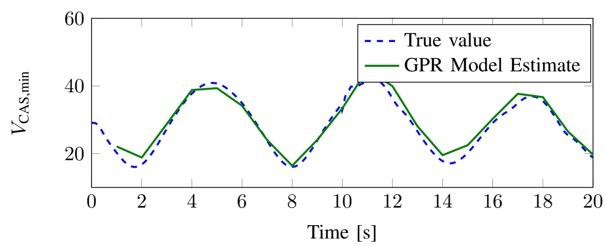

(a) Minimum calibrated airspeed envelope estimate

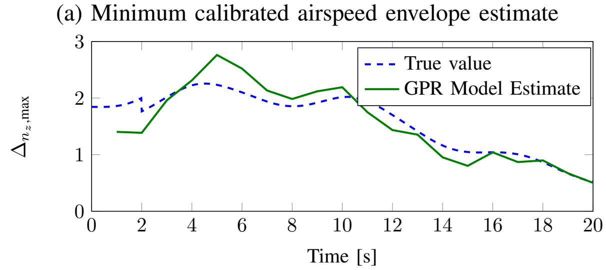

(b) Maximum load factor envelope estimate

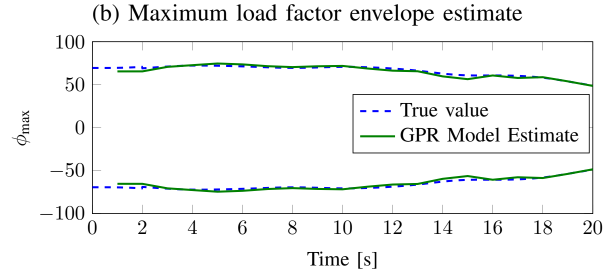

(c) Maximum bank angle envelope estimate

Fig. 11: Flight envelope estimate by the proposed method, with a 1-second update interval.

Numerical examples on aircraft icing and impairment conditions show that the GPR model effectively learns and infers the up-to-date shape of the lift curve, and the learning is more effective as more scattered data are available. Estimation of the flight envelope is further successfully validated under the NASA GTM wingtip loss damage condition.

While there is still research to be done, including the estimation of the flight path angle and pitch attitude envelopes using the drag coefficients as mentioned in reference [15], the effect of control surface damages or failures on the achievable envelope, and the utilisation of the uncertainty information in the GPR model.

ACKNOWLEDGEMENT

The authors were grateful to Zhihui Wang who kindly helped with the data processing.

REFERENCES

[1] Anon., "Statistical summary of commercial jet airplane accidents, worldwide operations, 19592015," tech. rep., Boeing Commercial Airplanes, Jan 2016.

[2] D. Bateman, "Some thoughts on reducing the risk of aircraft loss of control," in *AIAA Guidance, Navigation, and Control Conference*, p. 8139, 2010.

[3] Anon., "Safety report 2015," Tech. Rep. ISBN 978-92-9252-969-7, International Air Transport Association, April 2016. 52nd Edition.

[4] J. Wilborn and J. Foster, "Defining commercial transport loss-of-control: A quantitative approach," in *AIAA atmospheric flight mechanics conference and exhibit*, p. 4811, 2004.

[5] Anon., "A330 flight deck and systems briefing for pilots," Tech. Rep. STL 472.755/92 issue 4, Airbus, 1999.

[6] L. Tang, M. Roemer, J. Ge, A. Crassidis, J. Prasad, and C. Belcastro, "Methodologies for adaptive flight envelope estimation and protection," in *AIAA Guidance, Navigation, and Control Conference*, August 2009.

[7] J. Keller, R. McKillip, and S. Kim, "Aircraft flight envelope determination using upset detection and physical modeling methods," in *AIAA Guidance, Navigation, and Control Conference*, p. 6259, 2009.

[8] P. K. Menon, P. Sengupta, S. Vaddi, B.-J. Yang, and J. Kwan, "Impaired aircraft performance envelope estimation," *Journal of Aircraft*, vol. 50, no. 2, pp. 410–424, 2013.

[9] T. Lombaerts, S. Schuet, K. Wheeler, D. Acosta, and J. Kaneshige, "Robust maneuvering envelope estimation based on reachability analysis in an optimal control formulation," in *2013 Conference on Control and Fault-Tolerant Systems (SysTol)*, pp. 318–323, Oct 2013.

[10] S. Schuet, T. Lombaerts, D. Acosta, K. Wheeler, and J. Kaneshige, "An adaptive nonlinear aircraft maneuvering envelope estimation approach for online applications," in *AIAA Guidance, Navigation, and Control Conference*, p. 0268, 2014.

[11] T. Lombaerts, S. Schuet, D. Acosta, and J. Kaneshige, "On-line safe flight envelope determination for impaired aircraft," in *Advances in Aerospace Guidance, Navigation and Control*, pp. 263–282, Springer, 2015.

[12] T. Lombaerts, G. Looye, A. Seefried, M. Neves, and T. Bellmann, "Development and concept demonstration of a physics based adaptive flight envelope protection algorithm," *IFAC-PapersOnLine*, vol. 49, no. 5, pp. 248 – 253, 2016.

[13] C. E. Rasmussen and C. K. I. Williams, *Gaussian Processes for Machine Learning*. the MIT Press, 2006.

[14] M. Bragg, A. Broeren, and L. Blumenthal, "Iced-airfoil aerodynamics," *Progress in Aerospace Sciences*, vol. 41, no. 5, pp. 323 – 362, 2005.

[15] T. Lombaerts, G. Looye, J. Ellerbroek, and M. Rodriguez y Martin, "Design and piloted simulator evaluation of adaptive safe flight envelope protection algorithm," in *AIAA Guidance, Navigation, and Control Conference*, p. 0093, 2016.

[16] K. Cunningham, D. Cox, D. Murri, and S. Riddick, "A piloted evaluation of damage accommodating flight control using a remotely piloted vehicle," in *Proceedings of the 2011 AIAA Guidance, Navigation, and Control Conference*, (Portland, Oregon, USA), Aug 2011.